Materials Science in Semiconductor Processing 158 (2023) 107353

Contents lists available at ScienceDirect

Materials Science in Semiconductor Processing

journal homepage: www.elsevier.com/locate/mssp

Holding time effect on mechanical properties and protrusion behaviors of through silicon via copper under various annealing processes

Min Zhang [a], Fei Qin [a,b,**], Si Chen [c], Yanwei Dai [a,b,*], Yifan Jin [a], Pei Chen [a,b], Tong An [a,b], Yanpeng Gong [a,b]

[a] Institute of Electronics Packaging Technology and Reliability, Faculty of Materials and Manufacturing, Beijing University of Technology, Beijing, 100124, China
[b] Beijing Key Laboratory of Advanced Manufacturing Technology, Faculty of Materials and Manufacturing, Beijing University of Technology, Beijing, 100124, China
[c] Science and Technology on Reliability Physics and Application of Electronic Component Laboratory, China Electronic Product Reliability and Environmental Testing Research Institute, Guangzhou, 510610, China

ARTICLE INFO

Keywords:
Through Silicon Via copper (TSV-Cu)
Stress-strain constitutive curve
Protrusion
Annealing
Microstructure

ABSTRACT

The thermomechanical reliabilities of TSV based structures are closely affected by the protrusion deformation, stress-strain constitutive behavior and microstructure evolution of TSV-Cu under various thermal loadings. In this study, the stress-strain constitutive curves of TSV-Cu under various annealing conditions considering holding time effect are acquired by the nanoindentation test and finite element (FE) reverse analysis. The yielding softening in stress-strain curves is found if the holding time is less than 90 min. However, the stable stress-strain curves are obtained as holding time exceeds 90 min. Furthermore, the mechanisms of softening and stability in stress-strain curves are revealed by observing the microstructure evolution of TSV-Cu with a wide range of holding time. In addition, the relationships among protrusion height, constitutive curves as well as microstructure parameter of TSV-Cu with different annealing holding time are built. This study provides an intrinsic insight on the correlations of deformation, constitutive curves, and microstructure for TSV-Cu annealing processes considering holding time effect.

1. Introduction

Three-dimensional (3D) packaging based on copper filled through silicon via (TSV-Cu) technology can greatly improve the performance of integrated circuits, reduce power consumption, reduce weight and volume, which has been widely used in MEMS, mobile phones, memory products, CMOS image sensors, biological application equipment and other fields [1–3]. However, with the development of heterogeneity integration and the volume reduction of packaging, the requirement on design of crucial TSV interconnected structure becomes higher. Large initial residual stress accumulated in the fabrication processes could lead to the formation of voids, warpage, interface cracks and other reliability issues of interconnected structure [4]. Annealing treatment is an essential process to relieve the residual stress as well to stabilize the microstructure of TSV-Cu. However, multiple thermal loadings would cause TSV-Cu protrusions in the manufacturing process, resulting in deformation and damage of the back-end-of-line (BEOL) interconnected layers owing to the misfit in coefficients of thermal expansion between TSV-Cu and Si [5–12].

Understanding the constitutive behaviors is the prerequire to the reliability analysis. The traditional macro testing tools, including tensile, compressive and shearing test, are not available to acquire the mechanical parameters of TSV-Cu, due to a submicron length scale of interconnected structure. Therefore, Wang et al. [13] and Wu et al. [14] measured the elastic modulus and yield stress of TSV-Cu by micro pillar compressive testing system. However, the TSV-Cu micro pillar is surrounded by various dielectric materials, so exposing TSV-Cu micro pillar is expensive and time consuming by wet etching and focused iron beam (FIB) milling. Moreover, buckling issues during micro compressive testing would lead to measurement errors owing to the high aspect ratio

Abbreviations: MEMS, Micro-Electro-Mechanical Systems; CMOS, Complementary Metal-Oxide-Semiconductor.

* Corresponding author. Institute of Electronics Packaging Technology and Reliability, Faculty of Materials and Manufacturing, Beijing University of Technology, Beijing, 100124, China.
** Corresponding author. Institute of Electronics Packaging Technology and Reliability, Faculty of Materials and Manufacturing, Beijing University of Technology, Beijing, 100124, China.
E-mail addresses: qfei@bjut.edu.cn (F. Qin), ywdai@bjut.edu.cn (Y. Dai).

https://doi.org/10.1016/j.mssp.2023.107353
Received 14 November 2022; Received in revised form 17 January 2023; Accepted 20 January 2023
Available online 24 January 2023

of TSV-Cu pillar. Nanoindentation test can avoid above problems. Nanoindentation test is an effective way to measure elastic modulus and hardness of various engineering materials [15–18]. For example, nanoindentation tests were used by Heryanto et al. [19] and Okoro et al. [20] to measure the elastic modulus and hardness of TSV-Cu, the effects of the microstructure on the mechanical properties and the protrusion of TSV-Cu were also analyzed. Wang et al. [21,22] further explored the effects of various annealing temperatures on the TSV-Cu mechanical properties by nanoindentation test, and verified that the differences in mechanical properties among TSV-Cu, electroplated copper films and bulk copper were remarkable as the discrepancy of manufacturing process, size scale, microstructure and mechanical testing methods.

Inspired by the research of Dao et al. [23], the stress-strain curves for various engineering metals can be deduced from nanoindentation test combined with finite element (FE) reverse analysis. The principle is that materials possessing same elastic modulus, representative stress (σ_r) and representative strain (ε_r) should lead to same responses of indentation loading. Based on this method, stress-strain curves of various engineering materials such as sintered silver, aluminum, zirconium alloys etc. [16–18,23–27] were acquired. Noted that stress-strain curves of unannealed TSV-Cu have been reported in previous publications [28,29]. Recently, the effects of annealing temperatures and strain rates on the stress-strain curves of TSV-Cu were also investigated [30], it was verified that the yield stress reduced with increasing annealing temperatures, but heightened under the higher strain rate. The changing of yield stress was connected with the grain size according to the Hall-Petch theory [31]. Thus, the stress-strain curves of TSV-Cu can be optimized by microstructure. Hence, the reliabilities of TSV interconnected structure can be improved by reducing thermal stress and deformation during the manufacturing and service stage. However, the correlations of constitutive relations, microstructure evolution and protrusion deformation have not been fully clarified in the available literatures.

As is well known, the mechanisms of protrusions are mainly due to plastic strain, interfacial sliding and cracking, which are influenced by residual stress, microstructure, and interfacial mechanical property. The residual stress, interface strength and microstructure of TSV-Cu have been studied by experiments [14,32–38]. Furthermore, experimental or numerical methods were adopted to elucidate the protrusion mechanism, which is beneficial to control the protrusion of TSV-Cu under annealing. For example, tapered TSV and Cu/Si interface with small roughness would alleviate the stress concentration of Cu/Si interface, which decreased protrusion and the integrity failures of Cu/Si interface [39,40]. The optimization of mechanical properties of dielectric layers such as insulators and barriers could minimize the thermal stress to ameliorate the TSV-Cu protrusion [41]. Smaller diameter and larger pitch distance of TSV-Cu should be designed to reduce the protrusions under thermal loading [42]. Otherwise, the grain size and texture greatly influenced protrusion behaviors of TSV-Cu under annealing processes [35,36]. It is worth noting that annealing processes can eliminate defects, reduce residual stress and stabilize the microstructure of TSV-Cu, which are indispensable parts in the manufacturing processes of TSV interconnected structure.

Finer grain size could be obtained by annealing processes, which is able to reduce the protrusions of TSV-Cu [43]. Deng et al. [44] observed that the protrusion height decreased, then increased as the heating rates increased from 1 °C/min to 15 °C/min. Yang et al. [45] explored the influencing mechanisms of slower heating rates on the protrusion, i.e., interface sliding occurred at 0.01 °C/min, dislocation glide arose at 0.05 °C/min, interfacial cracking happened at rapid heating rate. It was also observed that protrusions exaggerated as holding time prolonged. De Wolf et al. [46] observed that the protrusions of TSV-Cu was reduced in subsequent thermal loading after suffering longer annealing holding time. The above literatures confirmed that annealing processes have a significant influence on the protrusion magnitude and mechanisms. Nevertheless, the effects of annealing process on stress-strain curves of TSV-Cu have not been fully investigated.

In this paper, annealing processes with a wide range of holding time were adopted to anneal the TSV-Cu, and its effects on the constitutive relation, protrusion deformation and microstructure of TSV-Cu were investigated. The outline is as following. The annealing conditions and experimental methods were presented in Section 2. The determination procedure of the stress-strain constitutive curve was displayed in Section 3. Section 4 presents the results of protrusion, constitutive relation and microstructure evolution. Then, their relationships were built and microstructure effects on the variations of constitutive relations were analyzed in the Discussions. Lastly, the conclusions were drawn.

2. Experiments

2.1. Preparation of testing samples

12-inch Si wafer with thickness of 800 μm (provided by NCAP, China), was prepared to fabricate the TSV sample. Main steps of fabrication processes were as following: Firstly, the blind vias on the Si wafer were etched by Bosch process. Then, the SiO_2 insulator layer with thickness of 550 nm was fabricated with chemical vapor deposition. Next, the Ti barrier layer with thickness of 80 nm was fabricated with plasma enhanced chemical vapor deposition. Lastly, the copper filled the blind vias by electroplating process. TSV samples with high aspect ratio (10:1) were obtained, i.e., depth is 100 μm and diameter is 10 μm, respectively. The manufactured 12-inch TSV wafer was diced into 3 mm × 3 mm small samples. The overburdened layers of Cu, SiO_2, and Ti on sample surface were removed with sandpaper and alumina polishing slurry. The TSV-Cu vias were exposed on the surface without obvious scratches or stains.

2.2. Annealing treatment and protrusion measurement

Five kinds of holding time, i.e., 30 min, 60 min, 90 min, 120 min, 200 min, were adopted to investigate the influences of annealing holding times. The annealing temperature was fixed as 400 °C since this temperature was verified as an effective temperature to reduce the protrusion of TSV-Cu [45,47]. As for annealing conditions, the room temperature raised up to 400 °C at 5 °C/min in the vacuum furnace (TL 2000), then held for different holding time, followed with naturally cooling down to room temperature.

3D laser scanning microscope with 12 nm resolution (KEYENCE X200 series) was utilized to measure the subscale TSV-Cu protrusion height after various annealing conditions. It was worth noting that the initial height of unannealed TSV-Cu was different from others. Ignoring the initial height would lead to obvious errors in measuring the annealed protrusion heights. Thus, the protrusion height difference of a same TSV-Cu via before and after annealing was the actual protrusion value. At least five TSV-Cu via protrusion heights were measured to guarantee the reliable measurement data. Moreover, to evaluate the effectiveness of various holding time for lowering subsequent TSV-Cu protrusion under following thermal loading, these annealed TSV samples were performed a second annealing with a same condition. The second annealing condition was that the room temperature heated up to 400 °C at 5 °C/min, and kept for 30 min at the 400 °C, then cooled naturally. The second TSV-Cu protrusion heights after double annealing conditions were also recorded with the same measuring method.

2.3. Characterization of mechanical properties and microstructure

Nanoindentation test (Agilent G200) was carried out on the TSV-Cu top surface to obtain the mechanical properties of TSV-Cu. Prior to the nanoindentation test, the top surface of TSV-Cu was polished to avoid the influence of surface roughness. Berkovich indenter and continuous stiffness measurement (CSM) were adopted to acquire the curves of elastic modulus (E) versus displacement and hardness (H) versus

displacement. The strain rate and the maximum indentation displacement were set as 0.05 s^{-1} and 800 nm, respectively. At least five repeatable measurements for each annealing condition were performed to guarantee repeatability of measuring data.

The microstructures of TSV-Cu with different annealing holding time were characterized with scanning electron microscope (SEM), equipped with the Oxford "Symmetry" detector. Before microstructure characterization, chemical mechanical polishing (CMP) was used to prepare the axial cross-section of TSV-Cu, then ion milling method was conducted to obtain the stress-free cross-section. Carbon with thickness of 5 nm was sputtered on milled cross-sections to enhance the conductivity of the EBSD scanning. After that, microstructure parameters, such as grain size distribution, grain boundary types and local misorientation, were analyzed with Channel 5 software.

3. Determination of stress-strain curve

3.1. Power law stress-strain constitutive model

For metals, the stress-strain constitutive curves are generally described by power law relations presented as below:

$$\begin{cases} \sigma = E\varepsilon, \sigma < \sigma_y \\ \sigma = \sigma_y\left(1+\dfrac{E}{\sigma_y}\varepsilon_p\right)^n, \sigma > \sigma_y \end{cases} \quad (1)$$

where σ_y, ε_p, n and E, are yield stress, plastic strain, hardening exponent and elastic modulus, respectively. The constitutive curve (denoted by blue curve) is described in Fig. 1(a), where E can be directly obtained by the load versus displacement curve based on the nanoindentation test. It can be seen that the coordinate (σ_r, ε_r), consisting of representative stress (σ_r) and representative strain (ε_r), is a particular point at the plastic deformation stage of the constitutive curve. The equation of σ_r and σ_y is presented as below:

$$\sigma_r = \sigma_y\left(1+\frac{E}{\sigma_y}\varepsilon_r\right)^n \quad (2)$$

Fig. 1(b) displays the load versus displacement curve of TSV-Cu. The maximum indenter force (F_m) occurred at the maximum displacement (h_m) during the loading. The plastic deformation of TSV-Cu under the loading stage caused the residual displacement (h_r) after the unloading. In addition, the work $\boldsymbol{W}_t$ made during indenter loading stage is consisted of plastic work $\boldsymbol{W}_p$ and elastic work $\boldsymbol{W}_e$, which were induced by the plastic deformation of TSV-Cu in loading stage, and recovered by elastic deformation during the unloading stage, respectively. The $\boldsymbol{W}_p$ is denoted by the green area, and $\boldsymbol{W}_e$ is displayed by grey area.

3.2. Finite element modeling for reverse analysis

The σ_r, ε_r can be determined by FE reverse analysis [48,49]. Herein, the FE model of TSV-Cu nanoindentation test is shown in Fig. 2(a). Two-dimensional local model with width and height (35 μm×35 μm) was established. SiO_2 and Ti dielectric layers between TSV-Cu/Si interface were negligible. In addition, the Cu/Si interface is assumed perfectly bonded though shared nodes in the FE model. The symmetrical constrains were applied on the left and bottom edges. Bilinear axisymmetric reduced integration element with four nodes (CAX4R) was adopted in the modeling. The total element numbers were 7326. The diamond indenter was regarded as rigid material. The elastic modulus and Poisson's ratio were 140 GPa, and 0.25, referred as the material parameters of Si substrate. The elastic modulus of TSV-Cu was set according to experimental results, and Poisson's ratio was set as 0.3.

Determination processes of σ_r, ε_r and n are based on reverse analysis, summarizing as a flow chart depicted in Fig. 3. The detail steps are stated as following.

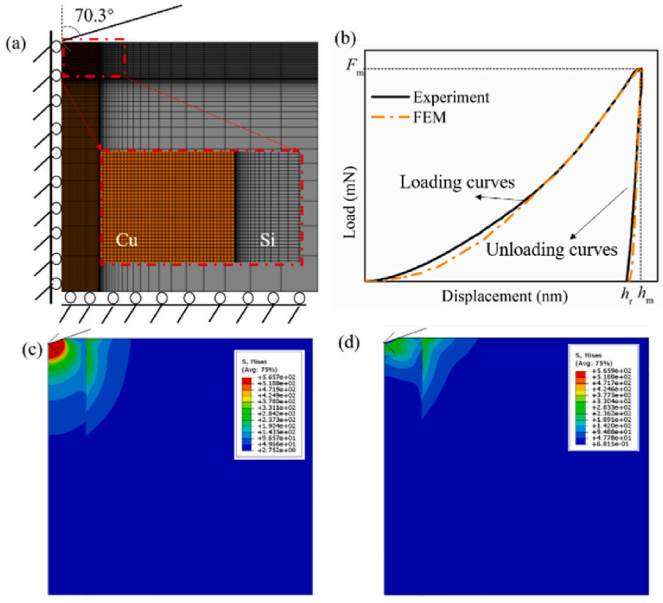

Fig. 2. Finite element modeling and load-displacement curve, (a) Finite element geometric model, (b) Load-displacement curves predicted by FEA, (c) Contour of von Mises stress at the maximum indenter displacement, (d) Contour of von Mises stress after the unloading.

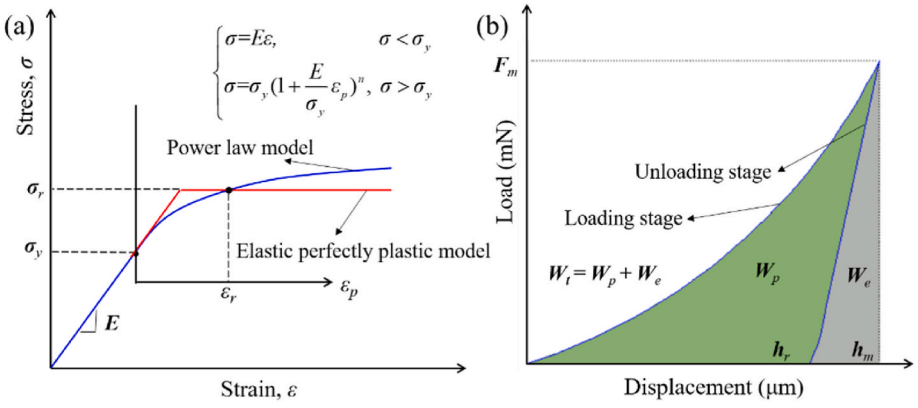

Fig. 1. Power law constitutive model and load versus displacement curve of nanoindentation test, (a) Power law constitutive curve, (b) Typical load versus displacement curve.

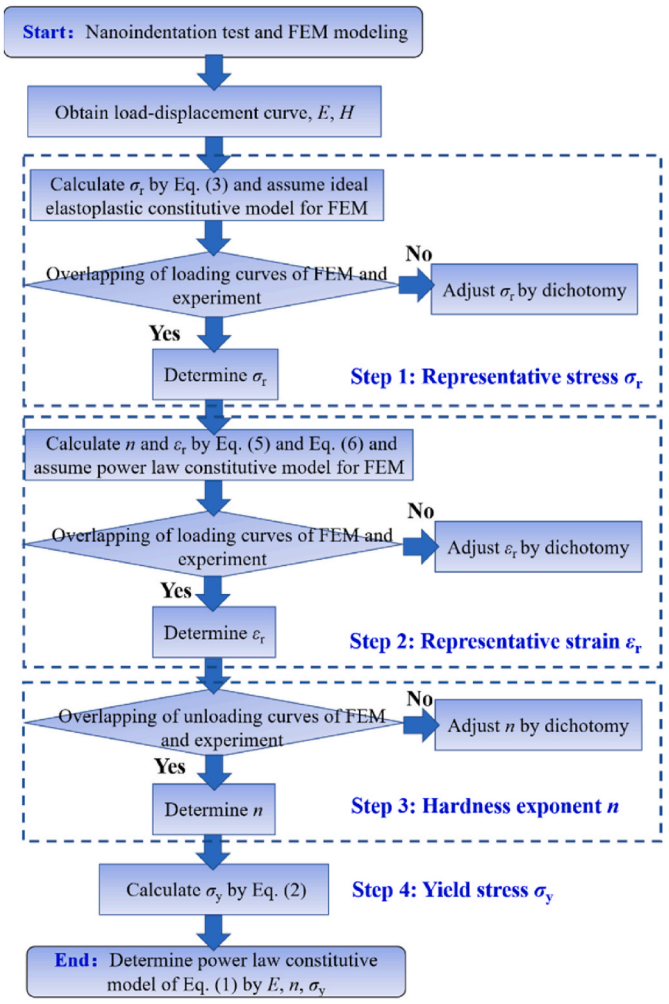

Fig. 3. Flowchart of FE reverse analysis to determine the power law constitutive equation.

Step 1: Determination of the representative stress σ_r. According to Pelletier et al. [50], the material with the same E and σ_r, would lead to similar indentation loading responses. Elastic-perfectly plastic constitutive curve of TSV-Cu was adopted in this step (denoted by red curve in Fig. 1(a)). The representative stress σ_r was regarded as the initial yield stress σ_y in the reverse analysis. The initial value of σ_r can be calculated from Eq. (3) according to Antunes et al. [51]:

$$\frac{E_r}{H} = 0.231\left(\frac{E_r}{\sigma_r}\right) + 4.910 \tag{3}$$

where H is the hardness, measured from the nanoindentation test. E_r is the reduced modulus, deduced from Eq. (4):

$$\frac{1}{E_r} = \frac{1-\nu^2}{E} + \frac{1-\nu_i^2}{E_i} \tag{4}$$

where E_i and ν_i are 1141 GPa and 0.07, respectively, taken as material parameters of the diamond indenter. The maximum displacement h_m in the loading and residual displacement h_r after the unloading were regarded as the loading to apply on the FE model. Dichotomy analysis was adopted by FEM to determine the final σ_r, enabling the overlapping of loading curves obtained from FE analysis and nanoindentation test. The relative error between F_m predicted by FE analysis and obtained from the nanoindentation experiment was less than 0.05%, which was the overlapping characteristics of the curves. The diagram of overlapping curves is presented in Fig. 2(b). The contour of von Mises stress at maximum displacement is exhibited as Fig. 2(c), and the contour of von Mises stress after unloading is displayed in Fig. 2(d). With the determined σ_r, the dimension function, shown as Eq. (5), was solved to deduce the hardening exponent n.

$$\Pi\left(\frac{\sigma_r}{E_r}, n\right) = \frac{h_r}{h_m} = A\left[\ln\left(\frac{\sigma_r}{E_r}\right)\right]^3 + B\left[\ln\left(\frac{\sigma_r}{E_r}\right)\right]^2 + C\ln\left(\frac{\sigma_r}{E_r}\right) + D \tag{5}$$

where the coefficients A, B, C and D are given as

$$\begin{cases} A = 0.010100n^2 + 0.0017639n - 0.0040837 \\ B = 0.14386n^2 + 0.018153n - 0.088198 \\ C = 0.59505n^2 + 0.034074n - 0.65417 \\ D = 0.58180n^2 - 0.088460n - 0.67290 \end{cases} \tag{6}$$

However, it was found that small variations of $\frac{\sigma_r}{E_r}$ would lead to large fluctuations of n. Therefore, the n will be adjusted after both σ_r and ε_r are determined.

Step 2: Determination of representative strain ε_r, by dichotomy analysis. The constitutive curve of TSV-Cu herein was power law constitutive curve in Fig. 1(a). The initial value of ε_r is calculated by Eq. (7) [52]:

$$\varepsilon_r = \exp\left(\frac{166.7}{E_r/\sigma_r + 177.3} - 3.91\right) \tag{7}$$

Step 3: Adjusting hardness exponent n. Antunes et al. [51] found that the unloading curve of the nanoindentation test is affected by n. Hence, n can be adjusted by ensuring the coincidence of the unloading curves in FE analysis and experiment.

Step 4: Determination of the yield stress σ_y. σ_y can be solved from Eq. (2) with the obtained E, σ_r, σ_r and n. In the end, the stress-strain curve is obtained by Eq. (1).

4. Results

4.1. Protrusions of TSV-Cu

Fig. 4 shows SEM images of TSV-Cu protrusion morphologies with various holding time, unannealed TSV-Cu morphology is corresponded to the holding time of 0 min, as shown in Fig. 4(a). As the holding time increases, the morphologies mainly exhibit edge, and center protrusions, displayed in Fig. 4(b–f). The edge protrusion was due to the great variations of grain size from the edge to the center of TSV-Cu, i.e., small

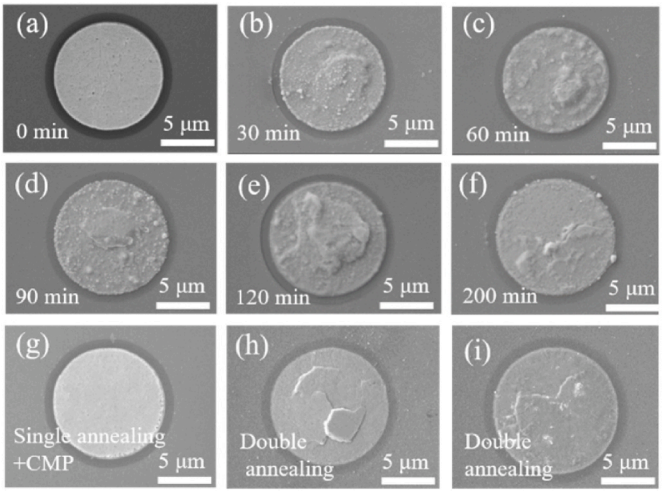

Fig. 4. Protrusion morphologies of TSV-Cu with various annealing holding time, (a) 0 min, (b) 30 min, (c) 60 min, (d) 90 min, (e) 120 min, (f) 200 min, (g) Single annealing + CMP, (h) and (i) Double annealing.

grains in the edge motivated more grain boundary diffusion [35]. The center protrusion was caused by the rotation of large grains [53]. After annealing for various holding time, TSV-Cu protrusions were removed by CMP, and the polished surface is shown in Fig. 4(g). Fig. 4(h and i) show the TSV-Cu morphologies after double annealing, the occurrence of center protrusions indicates the continuous rotation of large grains in the center of TSV-Cu.

Fig. 5 exhibits the TSV-Cu protrusion heights with various holding time. After single annealing, the protrusion height increases from 0.18 μm to 0.33 μm with prolonging the holding time to 120 min, then decreases to 0.24 μm under the holding time 200 min. After double annealing, the second protrusion height decreases from 0.14 μm to 0.05 μm as the single annealing holding time extends to 120 min, then increases to 0.09 μm under the single annealing holding time 200 min. The variation tendencies of the twice protrusion heights are opposite. In addition, the second protrusion height is greatly reduced, and the minimum protrusion height is 0.05 μm under the single annealing holding time of 120 min.

4.2. Constitutive behavior of TSV-Cu

Fig. 6(a and b) present the typical curves of E versus displacement, and H versus displacement for nanoindentation test under different annealing conditions, the stable data of E and H with indentation displacement of 600 nm–700 nm was averaged as the average values of E and H, respectively. Fig. 6(c) presents the average values of E after annealing. It is found that E keeps decreasing from 142.48 GPa to 105.53 GPa as holding time progresses under the single annealing. However, the average E fluctuates within 110 GPa–120 GPa under double annealing conditions. Fig. 6(d) shows average H after annealing. During the single annealing, the value of H deceases from 1.94 GPa to 1.10 GPa with increasing the holding time from 30 min to 90 min, then stables at 1 GPa. During the double annealing, the value of H reduces from 1.15 GPa to 1.07 GPa with the single annealing holding time increased from 30 min to 90 min, then keeps constant. It is suggested that double annealing barely changes the hardness of TSV-Cu after being annealed for 90 min. Table 1 presents the detailed values of E and H of TSV-Cu after various annealing holding time. Table 1 also gives the representative stress σ_r, strain ε_r, yield stress σ_y and hardening exponent n, obtaining through FE reverse analysis. It shows that σ_r and σ_y decrease, and n increases with the increase of holding time under single annealing, except the holding time of 200 min. As for double annealing, σ_r and σ_y also decrease, and n increases with the prolongation of holding time. In addition, the ε_r generally varies within 0.02–0.03.

Fig. 7 gives the stress-strain curves with various annealing conditions. After single annealing, the stress under the same strain decreases with the increase of the holding time (denoted by yellow line), except the holding time of 200 min, it is indicated that the softening occurs. After double annealing, all the curves stabilize around two curves of holding time 90 min and 120 min. It is suggested that double annealing results in slight variations of constitutive curves after annealing for 90 min.

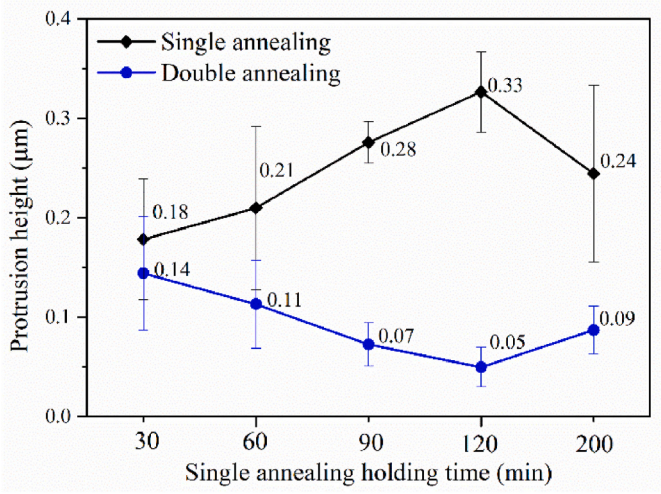

Fig. 5. Protrusion heights of TSV-Cu with various holding time.

4.3. Microstructure evolution

Fig. 8 presents the grain texture of TSV-Cu under various holding time. The annealed grains are enlarged and become equiaxed grains. Furthermore, the dominant orientations are <111> and <110>. Herein, the grains are classified as small, median and large grains according to diameters, i.e., $d < 1$ μm, 1 μm $< d <$ 4 μm and $d >$ 4 μm, respectively. The statistics of grain size are recorded in Table 2, the average grain size enlarges with the extension of single annealing holding time, except the holding time of 200 min. The reason is that the fraction of small grains is reduced, while the fraction of large grains is enlarged with the prolongation of holding time. After double annealing, the average grain size is about 3 μm, larger than that of annealed once.

Grain boundary types have remarkable effects on the mechanical properties and deformation behavior of materials. Fig. 9(a and b) present the distributions of grain boundaries. The low angle boundaries (LAGBs) with misorientation from 2° to 15°, and high angle boundaries with misorientation larger than 15°, are marked with grey lines and black lines, respectively. Other specific grain boundaries of coincident site lattice boundaries are included Σ3 (60°<111>) in red, Σ9 (38.94°<110>) in blue, Σ27a (31.58°<110>) in green and Σ27b (35.42°<210>) in yellow. These special grain boundaries possess lower freedom energy relative to random HAGBs, which is conducive to strengthening the mechanical properties [54,55]. It can be found that the total grain boundary numbers of annealed samples are reduced owing to grain growth. Σ3 is the most of the HAGBs, while the numbers of other grain boundary types are few. In addition, the distribution fraction of grain boundary types under single annealing is displayed in Fig. 9(c), the fraction of HAGBs increases with the single annealing holding time prolonged from 0 min to 60 min. However, the fraction of HAGBs reduces as the holding time exceeds 60 min. As shown in Fig. 9 (d), after double annealing, the fraction of HAGBs under double annealing is generally lower than that of HAGBs under single annealing.

The local misorientation can reflect the distributions of micro strain or dislocation density inside the grains. Generally, the micro strain or dislocation density would affect the thermodynamics state of grains under thermal mechanical loading. Fig. 10(a) displays the local misorientation distribution and its kernel average misorientation (KAM) of TSV-Cu under single annealing. Under single annealing with holding time 60 min, the KAM value decreases from 0.288 to 0.169 compared with that of unannealed grains. However, the KAM value heightens remarkably, even exceeds the initial value of unannealed grains with the holding time prolonged from 90 min to 120 min. In addition, the local misorientation distribution and the KAM value of TSV-Cu after double annealing are presented in Fig. 10(b). The KAM value increases relative to that of TSV-Cu annealed one time at holding time of 60 min and 90 min. Instead, the double annealing reduces the KAM values as the single annealing holding time reaches to 120 min. The variations of KAM values illustrate that micro strain and dislocation density exhibits a fluctuation tendency under various annealing holding time.

The softening behaviors of materials under annealing process are connected with the microstructure evolution. The distributions of recrystallized grains, subgrains and deformed grains after annealing are shown in Fig. 11(a and b). The grains with the KAM value exceeding 2° are deformed grains marked in red. Grains with the KAM value less than 2°, but whose misorientations among subgrains are larger than 2°, are subgrains marked in yellow [56]. Other remaining grains are recrystallized grains marked in blue. The fractions of the three kinds of grains

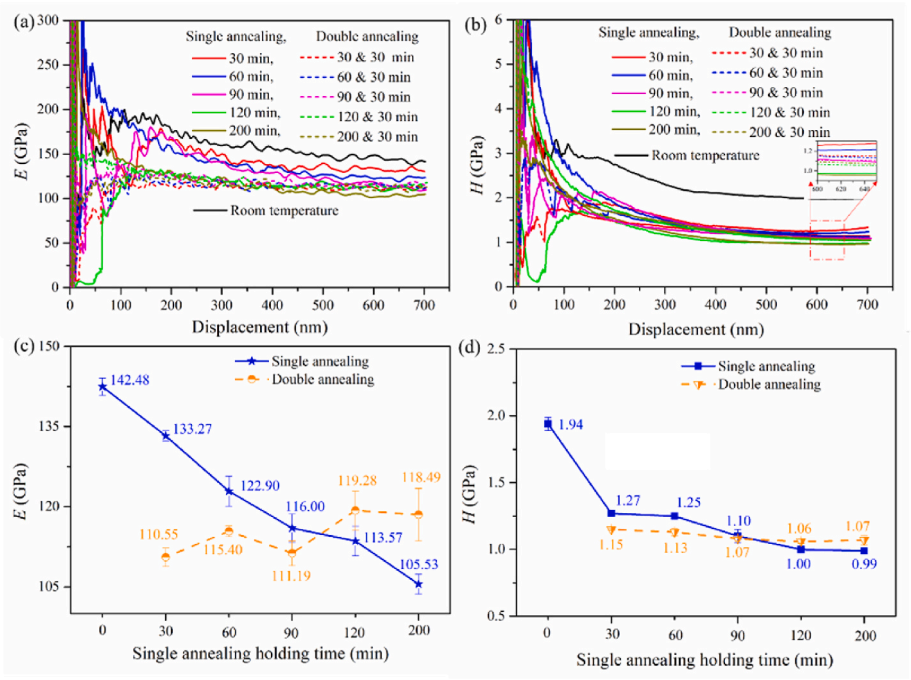

Fig. 6. *E* and *H* of TSV-Cu with various annealing holding time, (a) *E* versus displacement curves, (b) *H* versus displacement curves, (c) Average *E* after single and double annealing, (d) Average *H* after single and double annealing.

Table 1
Mechanical parameters of TSV-Cu from nanoindentation test and FE reverse.

Holding time (min)	Elastic modulus, *E* (GPa)	Hardness, *H* (GPa)	Representative stress, σ_r (MPa)	Representative strain, ε_r	Yield stress, σ_y (MPa)	Hardening exponent, *n*
0	142.48 ± 1.62	1.94 ± 0.05	478.98 ± 31.78	0.0284 ± 0.004	51.83 ± 6.67	0.5093 ± 0.0002
30	133.27 ± 0.95	1.27 ± 0.02	327.17 ± 10.27	0.0271 ± 0.001	26.09 ± 1.95	0.5121 ± 0.0001
60	122.00 ± 3.30	1.26 ± 0.03	319.50 ± 16.39	0.0283 ± 0.0001	25.78 ± 2.25	0.5126 ± 0.0001
90	116.00 ± 2.63	1.10 ± 0.05	248.34 ± 11.35	0.0294 ± 0.0001	15.63 ± 1.55	0.5134 ± 0.0001
120	113.57 ± 2.75	1.00 ± 0.02	239.37 ± 3.36	0.0301 ± 0.0008	13.85 ± 0.72	0.5170 ± 0.0001
200	105.53 ± 1.83	0.99 ± 0.02	273.93 ± 10.74	0.0262 ± 0.0006	21.32 ± 1.68	0.5239 ± 0.0001
30 & 30	110.55 ± 1.74	1.15 ± 0.01	254.52 ± 7.31	0.0292 ± 0.001	17.32 ± 0.52	0.5122 ± 0.0001
60 & 30	115.40 ± 1.04	1.13 ± 0.03	254.30 ± 8.87	0.0294 ± 0.001	16.67 ± 1.11	0.5126 ± 0.0001
90 & 30	111.03 ± 2.19	1.07 ± 0.01	238.13 ± 8.56	0.0285 ± 0.0008	15.44 ± 0.85	0.5134 ± 0.0001
120 & 30	119.28 ± 3.65	1.06 ± 0.02	235.94 ± 3.75	0.0292 ± 0.0005	13.13 ± 0.54	0.5172 ± 0.0003
200 & 30	118.49 ± 4.93	1.07 ± 0.04	232.62 ± 10.54	0.0293 ± 0.0009	11.85 ± 1.37	0.5243 ± 0.0002

are presented in Fig. 11(c–e). It can be found that the recrystallized fraction of unannealed grains is 70%, which indicates that most of grains have completed recrystallization before annealing. After single annealing, the recrystallized fraction increases from 70% to 85% with the holding time prolonged from 30 min to 90 min, but the fraction of subgrains deceases from 30% to 15%. With the holding time longer than 90 min, the recrystallized fraction reduces remarkably, and the fractions of subgrains and deformed grains heighten strikingly. After double annealing, the recrystallized fraction is generally lower than that of grains annealed one time with holding time of 60 min and 90 min. Meanwhile, the fractions of subgrains are higher than that of grains annealed one time. In addition, the fractions of deformed grains after double annealing are generally stable around 2.5%, except the double annealing condition 30 & 30 min.

5. Discussions

5.1. Relationships between protrusion, microstructure and mechanical properties

The nanoindentation technique can be applied for the mechanical property characterization of homogenous continuum with random orientations for the small volumed materials [57,58]. Furthermore, investigations showed that the mechanical properties on the top surface and cross-section of TSV-Cu with random orientations varied slightly, and the local top surface mechanical properties of TSV-Cu were closely correlated with the integral microstructure on the cross-section [19,30,59]. Herein, the relationships among protrusion deformation, top surface mechanical properties and integral microstructure on the cross-section are further discussed. As shown in the left part of Fig. 12 (a), under single annealing, both the protrusion height and average grain size generally increase with the holding time prolonged from 30 min to 120 min, then slightly reduce as the holding time extends to 200 min. As shown in the right part of Fig. 12(a), the variation tendencies of the yield stress, hardness and elastic modulus are opposite to that of the protrusion height and average grain size. That is because smaller grain leads to larger yield stress, on the basis of the Hall-Petch law. Moreover, the larger yield stress makes TSV-Cu harder to protrude by plastic deformation. In addition, with the enlarging of grain size, the hardness decreases, which is also explained by the Hall-Petch law. In fact, the decreased elastic modulus is influenced by mixed factors, including grain size, grain orientation, residual stress, and void defects [60–64].

However, the relationships among protrusion, microstructure and mechanical properties under double annealing conditions are different

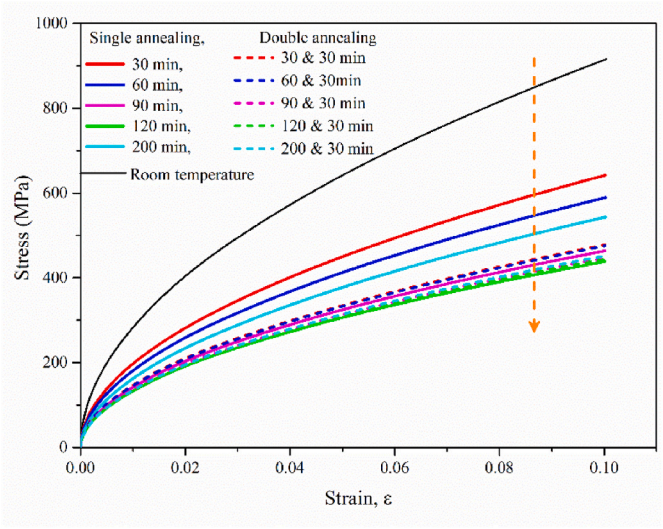

Fig. 7. The stress-strain curves of TSV-Cu under various conditions of holding time.

from that under single annealing, as shown in Fig. 12(b). The second protrusion height and yield stress reduce significantly compared with that under single annealing conditions, and generally exhibit a decreasing tendency with the extension of the single annealing holding time. The reduction mechanism of second protrusion height has been revealed [43], i.e., the second thermal loading contributed to the small increment of equivalent plastic strain and von Mises stress of TSV-Cu. Moreover, the average grain size and hardness tend to be stable, which also causes the reducing of the second protrusion height. Furthermore, elastic modulus exhibits fluctuation tendency. That could be connected with the grain orientation, i.e., elastic moduli corresponding to the <100> oriented and <111> oriented copper grains were 60 GPa, and 150 GPa, respectively [64].

5.2. *Effects of microstructure evolution on the softening in stress-strain curves of TSV-Cu*

The degree of softening was derived from the hardness data by the formula: $X_H = (H_\varepsilon - H_t)/(H_\varepsilon - H_0)$. Herein, H_0, H_ε, and H_t are the hardness values under various states, which were corresponded to the fully annealed state, the unannealed state, and the state of annealing for time t, respectively. Takayama et al. [65] fully annealed the Cu samples for long holding time to possess grains with comparable grain size to current investigation, and the measured H_0 was 0.5 GPa. As shown in Fig. 13, the blue curve and the diagram of microstructure evolution describe the softening characteristics during single annealing. The softening process is segmented with three stages. In Stage 1 with the holding time range 0–60 min, the softening is caused by the conventional static recovery (SRV), static recrystallization (SRX), and grain growth. During Stage 1, the new grains delineated by HAGBs are formed by recrystallization, which reduces the overall dislocation density. This interpretation is corresponded to the phenomena of the holding time range 0–60 min that the fraction of HAGBs increases in Fig. 9(c), KAM value decreases in Fig. 10(a), and the recrystallization fraction increases in Fig. 11(c). In stage 2 with the holding time range 60 min–120 min, the softening is mainly caused by the continuous grain growth. During this period, the dislocation density starts to increase, even higher than the initial dislocation density. The high density of dislocation generates subgrains inside the grains. Noted that subgrains in Fig. 13 are enclosed by original HAGBs denoted by black lines and newly formed LAGBs denoted by red lines. Therefore, the fraction of LAGBs increases in Fig. 9 (c), KAM value increases in Fig. 10(a), and a large number of subgrains forms in Fig. 11(d), which is also referred as discontinuous dynamic recrystallization (dDRX). In stage 3 with the holding time range 120 min–200 min, the softening value is basically stable. However, during this stage, the misorientation of LAGBs inside subgrains increases, enabling LAGBs to evolve into HAGBs and to form new small grains enclosed by HAGBs. Thus, the average grain size becomes finer, and the dislocations are relieved under the holding time of 200 min. Meanwhile, the fraction of LAGBs reduces in Fig. 9(c), and the KAM value also reduces in Fig. 10(a). It is speculated that the generation and annihilation of the dislocation density reached equilibrium, stabilizing the softening value.

The red curve depicts the softening process of double annealing. As the single annealing holding time is shorter than 90 min, the softening value of double annealing is larger than that of single annealing. The reason is mainly because the grain size continues to grow under double annealing. With the holding time longer than 90 min, the softening

Table 2
Average grain size and fraction distribution under various holding time.

Annealing holding time (min)	Average grain size d (μm)	Fraction of grain size distribution		
		Small (d < 1 μm)	Median (1 μm < d < 4 μm)	Large (d > 4 μm)
0	1.38	0.66	0.24	0.10
30	2.01	0.42	0.40	0.18
60	1.93	0.57	0.31	0.12
90	2.44	0.36	0.46	0.18
120	2.81	0.28	0.44	0.28
200	2.64	0.30	0.51	0.19
30 & 30	3.01	0.39	0.37	0.24
60 & 30	3.05	0.23	0.51	0.26
90 & 30	3.09	0.25	0.48	0.27
120 & 30	3.11	0.20	0.57	0.23
200 & 30	3.05	0.29	0.43	0.28

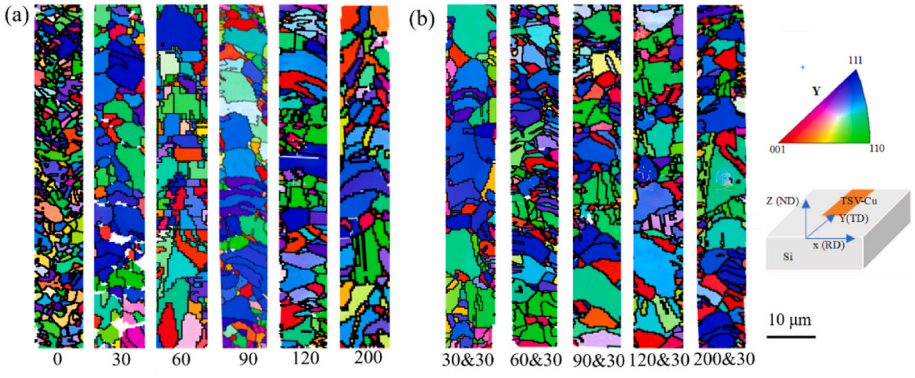

Fig. 8. EBSD maps of TSV-Cu with various holding time, (a) EBSD maps of TSV-Cu after single annealing, (b) EBSD maps of TSV-Cu after double annealing.

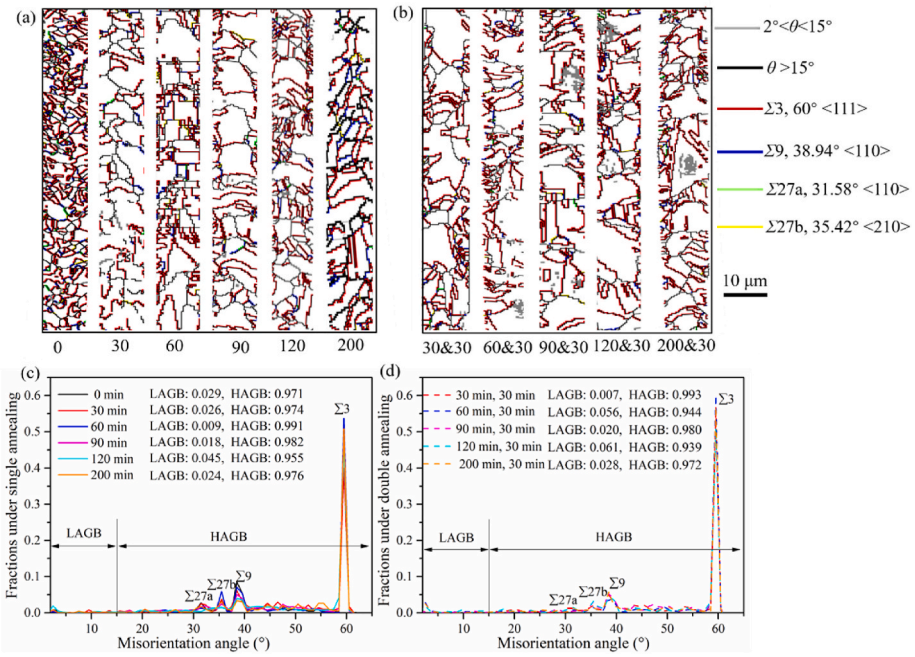

Fig. 9. Distributions and fractions of grain boundary types for TSV-Cu under various annealing processes, (a) Grain boundary types under single annealing, (b) Grain boundary types under double annealing, (c) Fractions of grain boundary types under single annealing, (d) Fractions of grain boundary types under double annealing.

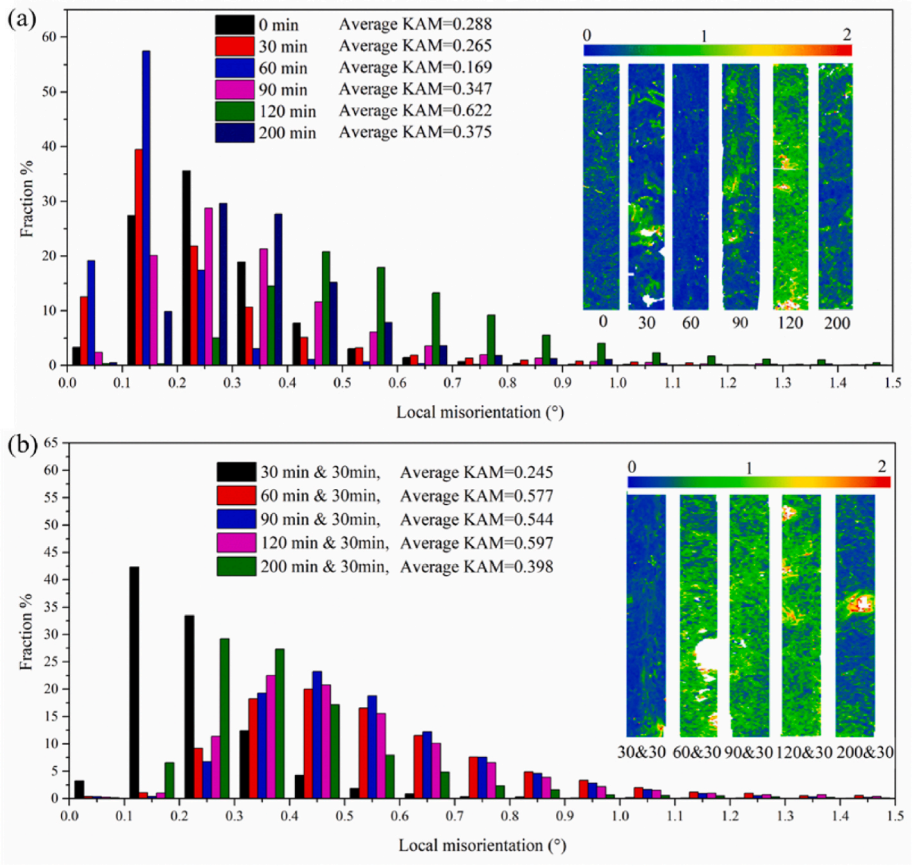

Fig. 10. Local misorientation distribution of TSV-Cu under different annealing holding time, (a) After single annealing, (b) After double annealing.

value is basically stable, but slightly smaller than that of single annealing. The main reason is that the fractions of LAGBs under double annealing increase relative to that under single annealing, leading to the strengthening effect on the hardness.

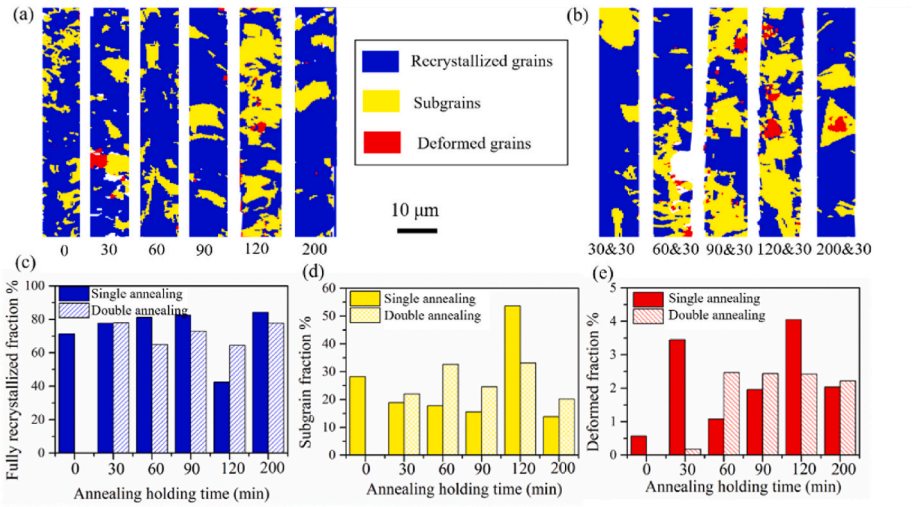

Fig. 11. Recrystallization distribution of TSV-Cu under various annealing holding time, (a) Recrystallization distribution after single annealing, (b) Recrystallization distribution after double annealing, (c) Fully recrystallized fraction, (d) Subgrain fraction, (e) Deformed fraction.

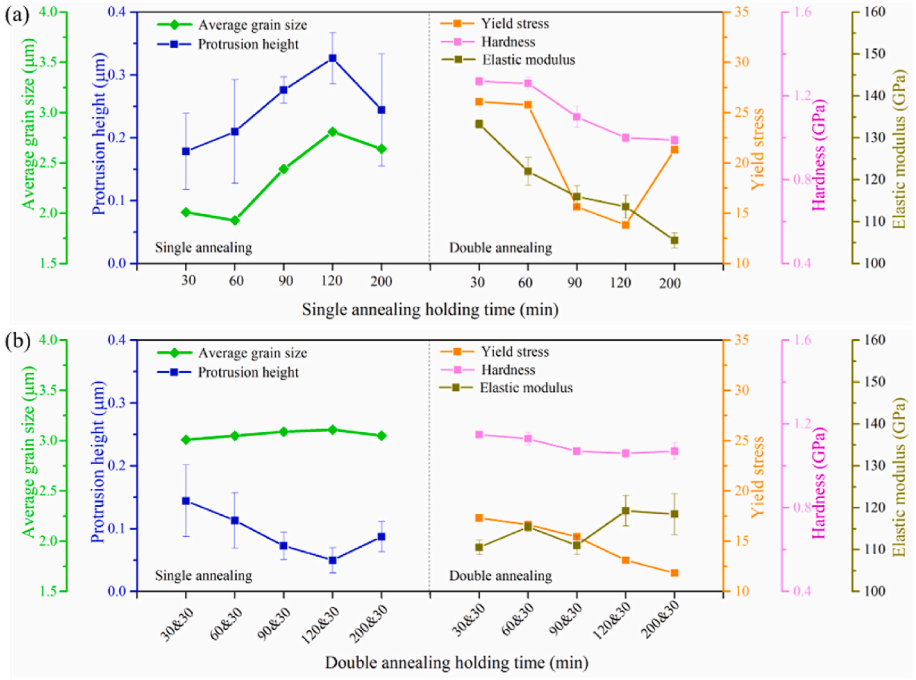

Fig. 12. Relationships among protrusion, microstructure and mechanical properties of TSV-Cu with various holding time, (a) Relationships under single annealing, (b) Relationships under double annealing.

6. Conclusions

In this paper, stress-strain curves of TSV-Cu under a wide range of holding time were obtained with nanoindentation test and FEM reverse analysis. The relationships among protrusion deformation, microstructure and constitutive behavior were built. In addition, the effects of microstructure on the softening mechanism of stress-strain curves were revealed. Conclusions are drawn as following.

1. The first protrusion height increased with prolonging holding time from 30 min to 120 min, then decreased slightly under the holding time of 200 min. However, the second protrusion height reduced firstly, followed by increasing after double annealing. It was worth noting that the second protrusion height was lower than first protrusion height.
2. The elastic modulus, hardness and yield stress generally decreased with the prolongation of single annealing holding time. Nevertheless, double annealing led to a slight fluctuation of elastic modulus, hardness and yield stress. Furthermore, the stress-strain curves softened with increasing the holding time from 30 min to 90 min, then stabilized as the holding time exceeded 90 min. Besides, the stability was not affected by double annealing conditions.
3. During single annealing, the average grain size generally increased with extending the holding time. During double annealing, the average grain size was stabilized around 3 μm. Meanwhile, the yield stress generally decreased with prolonging the holding time.
4. The softening in stress-strain curves is closely relevant to the microstructure evolution of TSV-Cu. During single annealing, the softening processes can be divided into three stages: Stage 1, with holding time 0–60 min, the softening was caused by conventional

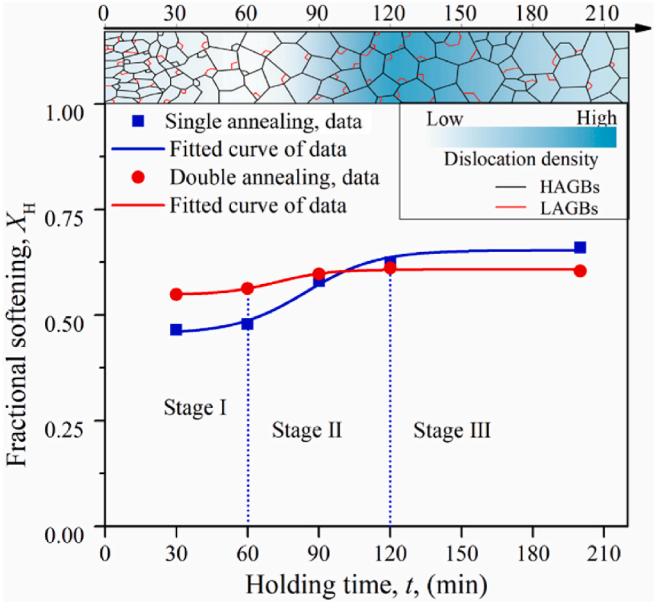

Fig. 13. Fractional softening versus holding time curves.

static recovery, static recrystallization and grain growth; Stage 2, with holding time 60 min–120 min, the softening was mainly resulted from the continuous grain growth, while discontinuous dynamic recrystallization occurred; Stage 3, with holding time 120 min–200 min, the softening value was basically unchanged, indicating that the balance of generation and annihilation of dislocations.

5. After double annealing, the softening value was higher than that under single annealing within the holding time of 90 min, due to the continuous grain growth. However, as the holding time exceeded 90 min, the softening value was lower than that under single annealing. That was because the second annealing promoted the generation of LAGBs, which slightly strengthened the hardness.

CRediT authorship contribution statement

Min Zhang: Writing – original draft, Visualization, Validation, Software, Methodology, Investigation, Data curation. **Fei Qin:** Supervision, Resources, Project administration, Methodology, Investigation, Funding acquisition, Writing – review & editing. **Si Chen:** Resources, Investigation, Funding acquisition, Writing – review & editing. **Yanwei Dai:** Writing – review & editing, Supervision, Methodology, Investigation, Conceptualization. **Yifan Jin:** Methodology, Investigation. **Pei Chen:** Investigation, Writing – review & editing. **Tong An:** Writing – review & editing. **Yanpeng Gong:** Writing – review & editing.

Declaration of competing interest

The authors declare that they have no known competing financial interests or personal relationships that could have appeared to influence the work reported in this paper.

Data availability

Data will be made available on request.

Acknowledgements

This work was supported by the National Natural Science Foundation of China (11672009, 61804032) and the Innovation and Entrepreneurship Leading Team Zengcheng under Grant No. 202102001. The authors also appreciated the assistance provided by HiSilicon Technologies CO., LIMITED during the study of this paper.

References

[1] J.P. Gambino, S.A. Adderly, J.U. Knickerbocker, An overview of through-silicon-via technology and manufacturing challenges, Microelecon. Eng. 135 (2015) 73–106, https://doi.org/10.1016/j.mee.2014.10.019.
[2] Y. Hu, L. Xiong, M. Li, T. Hang, Covalently formation of insulation and barrier layers in high aspect ratio TSVs, Appl. Surf. Sci. 573 (2022), https://doi.org/10.1016/j.apsusc.2021.151588.
[3] J. Wang, L. Ma, Y. Wang, Investigation on filling method and thermal reliability of Sn58Bi-TSV, Mater. Lett. 288 (2021), https://doi.org/10.1016/j.matlet.2021.129306.
[4] H. Guo, S. Cao, L. Li, X. Zhang, A review on the mainstream through-silicon via etching methods, Mater. Sci. Semicond. Process. 137 (2022), 106182, https://doi.org/10.1016/j.mssp.2021.106182.
[5] M. Song, Z. Wei, B. Wang, L. Chen, L. Chen, J.A. Szpunar, Study on copper protrusion of through-silicon via in a 3-D integrated circuit, Mater. Sci. Eng., A 755 (2019) 66–74, https://doi.org/10.1016/j.msea.2019.03.130.
[6] L. Hu, C.-H. Chen, S. Hsu, Y.C. Sheng, M.J. Lin, C.F. Lin, C.T. Yeh, C.H. Kuo, Optimization and characterization of the metal cap layout above through-silicon via to improve copper dishing and protrusion effect for the application of 3-D integrated circuits, IEEE Trans. Compon. Packag. Manuf. Technol. 8 (12) (2018) 2222–2226, https://doi.org/10.1109/tcpmt.2018.2858286.
[7] F. Qin, M. Zhang, Y. Dai, P. Chen, T. An, H. He, H. Zhang, J. Zheng, Optimization of TSV interconnects and BEOL layers under annealing process through fracture evaluation, Fatig. Fract. Eng. Mater. Struct. 43 (7) (2020) 1433–1455, https://doi.org/10.1111/ffe.13206.
[8] Y. Dai, M. Zhang, F. Qin, P. Chen, T. An, Effect of silicon anisotropy on interfacial fracture for three dimensional through-silicon-via (TSV) under thermal loading, Eng. Fract. Mech. 209 (2019) 274–300, https://doi.org/10.1016/j.engfracmech.2019.01.030.
[9] C. Rao, T. Wang, Y. Peng, J. Cheng, Y. Liu, S.K. Lim, X. Lu, Residual stress and pop-out simulation for TSVs and contacts in via-middle process, IEEE Trans. Semicond. Manuf. 30 (2) (2017) 143–154, https://doi.org/10.1109/tsm.2017.2688498.
[10] Y. Chen, W. Su, H.-Z. Huang, P. Lai, X.-L. Lin, S. Chen, Stress evolution mechanism and thermo-mechanical reliability analysis of copper-filled TSV interposer, Eksploatacja i Niezawodnosc - Maintenance and Reliab 22 (4) (2020) 705–714, https://doi.org/10.17531/ein.2020.4.14.
[11] E. Kim, S. Choi, S. Jeon, H. Seo, J.-i. Cho, Development of novel multi-selective slurry with mechanically driven etching for through silicon via chemical mechanical polishing, Mater. Sci. Semicond. Process. 152 (2022), 107025, https://doi.org/10.1016/j.mssp.2022.107025.
[12] S. Wang, H. Zhang, Z. Tian, T. Liu, Y. Sun, Y. Zhang, F. Dong, S. Liu, Optimization of Cu protrusion of wafer-to-wafer hybrid bonding for HBM packages application, Mater. Sci. Semicond. Process. 152 (2022), https://doi.org/10.1016/j.mssp.2022.107063.
[13] H. Wang, P. Cheng, H. Wang, R. Liu, L. Sun, Q. Rao, Z. Wang, T. Gu, G. Ding, Effect of current density on microstructure and mechanical property of Cu micro-cylinders electrodeposited in through silicon vias, Mater. Char. 109 (2015) 164–172, https://doi.org/10.1016/j.matchar.2015.09.029.
[14] C. Wu, R. Huang, K.M. Liechti, Characterizing interfacial sliding of through-silicon-via by nano-indentation, IEEE Trans. Device Mater. Reliab. 17 (2) (2017) 355–363, https://doi.org/10.1109/tdmr.2017.2681580.
[15] W.C. Oliver, G.M. Pharr, An improved technique for determining hardness and elastic modulus using load and displacement sensing indentation experiments, J. Mater. Res. 7 (6) (1992) 1564–1583, https://doi.org/10.1557/JMR.1992.1564.
[16] X. Long, Q.P. Jia, Z. Li, S.X. Wen, Reverse analysis of constitutive properties of sintered silver particles from nanoindentations, Int. J. Solid Struct. 191–192 (2020) 351–362, https://doi.org/10.1016/j.ijsolstr.2020.01.014.
[17] M. Isik, N.M. Gasanly, F.A. Rustamov, Determination of mechanical properties of Bi12TiO20 crystals by nanoindentation, Mater. Sci. Semicond. Process. 140 (2022), https://doi.org/10.1016/j.mssp.2021.106389.
[18] R. Li, C. Mo, Y. Liao, Mechanical properties of U-Cu intermetallic compound measured by nanoindentation, Materials 11 (11) (2018), https://doi.org/10.3390/ma11112215.
[19] A. Heryanto, W.N. Putra, A. Trigg, S. Gao, W.S. Kwon, F.X. Che, X.F. Ang, J. Wei, R. I Made, C.L. Gan, K.L. Pey, Effect of copper TSV annealing on via protrusion for TSV wafer fabrication, J. Mater. Sci. 41 (9) (2012) 2533–2542, https://doi.org/10.1007/s11664-012-2117-3.
[20] C. Okoro, K. Vanstreels, R. Labie, O. Lühn, B. Vandevelde, B. Verlinden, D. Vandepitte, Influence of annealing conditions on the mechanical and microstructural behavior of electroplated Cu-TSV, J. Micromech. Microeng. 20 (4) (2010), https://doi.org/10.1088/0960-1317/20/4/045032.
[21] H. Wang, H. Wang, P. Cheng, R. Liu, Z. Wang, G. Ding, Microstructure and hardness of electrodeposited copper microcylinders in through-silicon via by direct current power, Micro & Nano Lett. 11 (6) (2016) 308–310, https://doi.org/10.1049/mnl.2015.0519.
[22] H. Wang, P. Cheng, S. Wang, H. Wang, T. Gu, J. Li, X. Gu, G. Ding, Effect of thermal treatment on the mechanical properties of Cu specimen fabricated using electrodeposition bath for through-silicon-via filling, Microelecon. Eng. 114 (2014) 85–90, https://doi.org/10.1016/j.mee.2013.09.007.
[23] M. Dao, N. Chollacoop, K.J. Van Vliet, T.A. Venkatesh, S. Suresh, Computational modeling of the forward and reverse problems in instrumented sharp indentation,

Acta Mater. 49 (19) (2001) 3899–3918, https://doi.org/10.1016/S1359-6454(01)00295-6.
[24] X. Long, B. Hu, Y. Feng, C. Chang, M. Li, Correlation of microstructure and constitutive behaviour of sintered silver particles via nanoindentation, Int. J. Mech. Sci. 161–162 (2019), https://doi.org/10.1016/j.ijmecsci.2019.105020.
[25] M.K. Khan, S.V. Hainsworth, M.E. Fitzpatrick, L. Edwards, A combined experimental and finite element approach for determining mechanical properties of aluminium alloys by nanoindentation, Comput. Mater. Sci. 49 (4) (2010) 751–760, https://doi.org/10.1016/j.commatsci.2010.06.018.
[26] H. Wang, J. Thomas, M.A. Okuniewski, V. Tomar, Constitutive modeling of δ-phase zircaloy hydride based on strain rate dependent nanoindentation and nano-scale impact dataset, Int. J. Plast. 133 (2020), https://doi.org/10.1016/j.ijplas.2020.102787.
[27] H. Li, J. Chen, Q. Chen, M. Liu, Determining the constitutive behavior of nonlinear visco-elastic-plastic PMMA thin films using nanoindentation and finite element simulation, Mater. Des. 197 (2021), https://doi.org/10.1016/j.matdes.2020.109239.
[28] W. Wei, Q. Fei, A. Tong, C. Pei, Experimental and numerical investigation of mechanical properties of electroplating copper filled in through silicon vias, IEEE Trans. Compon. Packag. Manuf. Technol. 6 (1) (2016) 23–30, https://doi.org/10.1109/tcpmt.2015.2506202.
[29] W. Wu, F. Qin, T. An, P. Chen, A study of creep behavior of TSV-Cu based on nanoindentaion creep test, J. Mech. 32 (6) (2016) 717–724, https://doi.org/10.1017/jmech.2016.55.
[30] Y. Li, P. Chen, F. Qin, T. An, Y. Dai, M. Zhang, Y. Jin, Constitutive modelling of annealing behavior in through silicon vias-copper, Mater. Char. 179 (2021), https://doi.org/10.1016/j.matchar.2021.111359.
[31] N. Hansen, Hall–Petch relation and boundary strengthening, Scripta Mater. 51 (8) (2004) 801–806, https://doi.org/10.1016/j.scriptamat.2004.06.002.
[32] A.S. Budiman, H.A.S. Shin, B.J. Kim, S.H. Hwang, H.Y. Son, M.S. Suh, Q.H. Chung, K.Y. Byun, N. Tamura, M. Kunz, Y.C. Joo, Measurement of stresses in Cu and Si around through-silicon via by synchrotron X-ray microdiffraction for 3-dimensional integrated circuits, Microelectron, Reliab 52 (3) (2012) 530–533, https://doi.org/10.1016/j.microrel.2011.10.016.
[33] C. Okoro, L.E. Levine, R. Xu, Y. Obeng, Experimental measurement of the effect of copper through-silicon via diameter on stress buildup using synchrotron-based X-ray source, J. Mater. Sci. 50 (18) (2015) 6236–6244, https://doi.org/10.1007/s10853-015-9184-9.
[34] S. Chen, Y.F. En, G.Y. Li, Z.Z. Wang, R. Gao, R. Ma, L.X. Zhang, Y. Huang, An ion beam layer removal method of determining the residual stress in the as-fabricated TSV-Cu/TiW/SiO2/Si interface on a nanoscale, Microelectron. Reliab. 112 (2020), https://doi.org/10.1016/j.microrel.2020.113826.
[35] T. An, F. Qin, S. Chen, P. Chen, The effect of the diffusion creep behavior on the TSV-Cu protrusion morphology during annealing, J. Mater. Sci. Mater. Electron. 29 (19) (2018) 16305–16316, https://doi.org/10.1007/s10854-018-9720-x.
[36] S.-H. Kim, H.-J. Lee, D. Josell, T.P. Moffat, Bottom-up Cu filling of annular through silicon vias: microstructure and texture, Electrochim. Acta 335 (2020), https://doi.org/10.1016/j.electacta.2020.135612.
[37] C. Wu, C. Wei, Y. Li, In situ mechanical characterization of the mixed-mode fracture strength of the Cu/Si interface for TSV structures, Micromachines 10 (2) (2019), https://doi.org/10.3390/mi10020086.
[38] D. Jeong, R. Abdur, Y.-C. Joo, J.-i. Jang, P.R. Cha, J. Kim, K.-S. Min, J. Lee, Effects of interfacial layer-by-layer nanolayers on the stability of the Cu TSV: diffusion barrier, adhesion, conformal coating, and mechanical property, Mater. Sci. Semicond. Process. 83 (2018) 33–41, https://doi.org/10.1016/j.mssp.2018.04.008.
[39] A. Eslami Majd, I.H. Jeong, J.P. Jung, N.N. Ekere, Cu protrusion of different through-silicon via shapes under annealing process, J. Mater. Eng. Perform. 30 (6) (2021) 4712–4720, https://doi.org/10.1007/s11665-021-05775-4.
[40] S. Chen, Z. Wang, Y. En, Y. Huang, F. Qin, T. An, The experimental analysis and the mechanical model for the debonding failure of TSV-Cu/Si interface, Microelectron. Reliab. 91 (2018) 52–66, https://doi.org/10.1016/j.microrel.2018.08.005.
[41] Y. Zare, Y. Sasajima, J. Onuki, A novel lining method for eliminating plastic deformation and protrusion of copper in Cu-TSV using FEM analysis, J. Mater. Sci. 49 (6) (2020) 3692–3700, https://doi.org/10.1007/s11664-020-08076-z.
[42] G. Jalilvand, O. Ahmed, N. Dube, T. Jiang, The effect of pitch distance on the statistics and morphology of through-silicon via extrusion, IEEE Trans. Compon. Packag. Manuf. Technol. 11 (6) (2021) 883–891, https://doi.org/10.1109/tcpmt.2021.3078772.
[43] M. Zhang, F. Qin, S. Chen, Y. Dai, P. Chen, T. An, Protrusion of through-silicon-via (TSV) copper with double annealing processes, J. Mater. Sci. 51 (5) (2022) 2433–2449, https://doi.org/10.1007/s11664-022-09503-z.
[44] Q. Deng, L. Huang, J. Shang, M. Li, Study on TSV-Cu Protrusion under Different Annanling Condition and Optimization, 2016 17th International Conference on Electronic Packaging Technology, ICEPT), Wuhan, China, 2016, pp. 380–383.
[45] H. Yang, T.-K. Lee, L. Meinshausen, I. Dutta, Heating rate dependence of the mechanisms of copper pumping in through-silicon vias, J. Mater. Sci. 48 (1) (2018) 159–169, https://doi.org/10.1007/s11664-018-6805-5.
[46] I. De Wolf, K. Croes, O. Varela Pedreira, R. Labie, A. Redolfi, M. Van De Peer, K. Vanstreels, C. Okoro, B. Vandevelde, E. Beyne, Cu pumping in TSVs: effect of pre-CMP thermal budget, Microelectron. Reliab. 51 (9–11) (2011) 1856–1859, https://doi.org/10.1016/j.microrel.2011.06.003.
[47] C. Okoro, C. Huyghebaert, J. Van Olmen, R. Labie, K. Lambrinou, B. Vandevelde, E. Beyne, D. Vandepitte, E. Zschech, S. Ogawa, P.S. Ho, Elimination of the axial deformation problem of Cu-TSV in 3D integration, AIP Conf. Proc. 1300 (1) (2010) 214–220, https://doi.org/10.1063/1.3527128.
[48] Y.-T. Cheng, C.-M. Cheng, Scaling approach to conical indentation in elastic-plastic solids with work hardening, J. Appl. Phys. 84 (3) (1998) 1284–1291, https://doi.org/10.1063/1.368196.
[49] K. Tunvisut, N. O'Dowd, E.P. Busso, Use of scaling functions to determine mechanical properties of thin coatings from microindentation tests, Int. J. Solid Struct. 38 (2) (2001) 335–351, https://doi.org/10.1016/S0020-7683(00)00017-2.
[50] H. Pelletier, Predictive model to estimate the stress–strain curves of bulk metals using nanoindentation, Tribol. Int. 39 (7) (2006) 593–606, https://doi.org/10.1016/j.triboint.2005.03.019.
[51] J. Antunes, J. Fernandes, L. Menezes, B. Chaparro, A new approach for reverse analyses in depth-sensing indentation using numerical simulation, Acta Mater. 55 (1) (2007) 69–81, https://doi.org/10.1016/j.actamat.2006.08.019.
[52] J. Lee, C. Lee, B. Kim, Reverse analysis of nano-indentation using different representative strains and residual indentation profiles, Mater. Des. 30 (9) (2009) 3395–3404, https://doi.org/10.1016/j.matdes.2009.03.030.
[53] X. Zhao, L. Ma, Y. Wang, F. Guo, Mechanism of the local Cu protrusion in Cu-filled through silicon vias under heat treatment, J. Mater. Sci. 48 (1) (2018) 152–158, https://doi.org/10.1007/s11664-018-6803-7.
[54] L. Lu, Y. Shen, X. Chen, L. Qian, K. Lu, Ultrahigh strength and high electrical conductivity in copper, Science 304 (5669) (2004) 422–426, https://doi.org/10.1126/science.1092905.
[55] P. Zhang, Z.J. Zhang, L.L. Li, Z.F. Zhang, Corrigendum to "Twin boundary: stronger or weaker interface to resist fatigue cracking?", Scripta Mater. 67 (9) (2012) https://doi.org/10.1016/j.scriptamat.2012.08.003.
[56] G.K. Padhy, C.S. Wu, S. Gao, Subgrain formation in ultrasonic enhanced friction stir welding of aluminium alloy, Mater. Lett. 183 (2016) 34–39, https://doi.org/10.1016/j.matlet.2016.07.033.
[57] S.-H. Kim, Y.-C. Kim, S. Lee, J.-Y. Kim, Evaluation of tensile stress-strain curve of electroplated copper film by characterizing indentation size effect with a single nanoindentation, Met. Mater. Int. 23 (2017) 76–81, https://doi.org/10.1007/s12540-017-6461-y.
[58] X.-w. Feng, J. Xie, W.-y. Xue, Y.-f. Shen, H.-b. Wang, Z.-y. Liu, Microstructure and nanoindentation hardness of shot-peened ultrafine-grained low-alloy steel, J. Iron Steel Res. 26 (2018) 472–482, https://doi.org/10.1007/s42243-018-0061-z.
[59] M. Zhang, F. Qin, S. Chen, Y.W. Dai, Y.F. Jin, P. Chen, T. An, Y.P. Gong, Effect of capped Cu layer on protrusion behaviors of through silicon via copper (TSV-Cu) under double annealing conditions: comparative study, IEEE Trans. Dev. Mater. Relia. Online (2022), https://doi.org/10.1109/TDMR.2022.3232128.
[60] K. Zhou, B. Liu, Y. Yao, K. Zhong, Effects of grain size and shape on mechanical properties of nanocrystalline copper investigated by molecular dynamics, Mater. Sci. Eng., A 615 (2014) 92–97, https://doi.org/10.1016/j.msea.2014.07.066.
[61] M. Faheem, R.R. Giridharan, Y. Liang, P. van Der Heide, Micro-XRD characterization of a single copper filled through-silicon via, Mater. Lett. 161 (2015) 391–394, https://doi.org/10.1016/j.matlet.2015.08.140.
[62] H. Kim, H. Jeon, D.-J. Lee, J.-Y. Kim, Surface residual stress in amorphous SiO2 insulating layer on Si substrate near a Cu through-silicon via (TSV) investigated by nanoindentation, Mater. Sci. Semicond. Process. 135 (2021), https://doi.org/10.1016/j.mssp.2021.106153.
[63] Y.-H. Lee, D. Kwon, Measurement of residual-stress effect by nanoindentation on elastically strained (100) W, Scripta Mater. 49 (5) (2003) 459–465, https://doi.org/10.1016/s1359-6462(03)00290-2.
[64] A. Basavalingappa, J.R. Lloyd, Effect of microstructure and anisotropy of copper on reliability in nanoscale interconnects, IEEE Trans. Device Mater. Reliab. 17 (1) (2017) 69–79, https://doi.org/10.1109/tdmr.2017.2655459.
[65] A. Takayama, X. Yang, H. Miura, T. Sakai, Continuous static recrystallization in ultrafine-grained copper processed by multi-directional forging, Mater. Sci. Eng., A 478 (1–2) (2008) 221–228, https://doi.org/10.1016/j.msea.2007.05.115.